Appendix A

The following paper was submitted to the Journal of Hydraulic Engineering and was accepted for publication on March 15, 2021.

Wahl, Tony L., Christopher C. Shupe, H. Dzafo & E. Dzaferovic. 2021. Surface tension effects on the discharge capacity of Coanda-effect screens. *Journal of Hydraulic Engineering*. DOI: 10.1061/(ASCE)HY.1943-7900.0001902

Pre-print of Wahl et al. (2021). DOI: 10.1061/(ASCE)HY.1943-7900.0001902

Surface Tension Effects on the Discharge Capacity of Coanda-Effect Screens

Tony L. Wahl, P.E., M. ASCE[1], Christopher C. Shupe[2], Hajrudin Dzafo[3], Ejub Dzaferovic[4]

ABSTRACT

Coanda-effect screens exclude coarse and fine debris from a variety of water intakes. Water overflows an inclined wedge-wire screen with tilted wires that shear high velocity flow from the bottom of the water column. The screens hydraulically self-clean, making them ideal for remote, nonpowered sites. Flow conditions vary widely over the length of most screens. Previous testing related flow capacity to gravitational, surface tension, and viscous forces, but the range of flow conditions was limited versus potential applications. Here, small sections of prototype-scale screens were tested at varying slopes, and discharge coefficients were related to Froude and Weber numbers. Tests with variable water temperatures proved screen performance is independent of Reynolds number and viscosity but depends strongly on surface tension. Several screen geometries (i.e., wire size, shape, and slot size) were tested, and the performance of all screens could be modeled with power curve functions of the Weber number modified by the Froude number. Individual screens exhibited some unique performance characteristics, but 10 of the 13 screens could be effectively modeled as a group.

INTRODUCTION

Coanda-effect screens have been used worldwide since the 1980s for screening of organic debris, trash, sediment, and aquatic organisms from a variety of water intakes (Finch and Strong 1983; Strong and Ott 1988). Small hydropower intakes were a common application cited in a review of case studies (Wahl 2003). Fontein (1965) described the use of similar screens for solids removal in mining applications as early as 1955. Esmond (2012) described the use of Coanda-effect screens for applications related to stormwater management, and May (2015) conducted laboratory tests to evaluate the effectiveness of the screens for sediment removal at water system intakes in rural areas of developing countries. Nøvik et al. (2014) studied hydropower applications in cold climates affected by frazil ice and found the screens to be resilient against ice blockage in all but the most extreme conditions and quick to clear after ice blockage events.

A typical Coanda-effect screen structure is shown schematically in Fig. 1 (Wahl 2001). The screen panel is installed downstream from the crest of an overflow weir so that high-velocity supercritical flow passes across the screen surface. An acceleration plate leads the flow tangentially onto the screen. The screen panel is composed of wedge wire, with the individual wires oriented perpendicular to the flow direction. Each wire is tilted a few degrees downstream on its axis so that the leading edges of the wires form a series of water-shearing offsets projecting into the flow. The Coanda effect causes flow to attach to the top surface of each wire so that the flow in the immediate vicinity of the wires is parallel to the wire surfaces instead of

[1] Technical Specialist, Bureau of Reclamation, Hydraulics Laboratory, Denver, Colorado, USA, <twahl@usbr.gov>
[2] Hydraulic Engineer, Bureau of Reclamation, Hydraulics Laboratory, Denver, Colorado, USA
[3] Assistant Professor, International Burch University, BOSNIA-HERZEGOVINA
[4] Professor, University of Sarajevo, BOSNIA-HERZEGOVINA

the overall screen surface. At the trailing edge of each wire the flow detaches cleanly from the wire and upon striking the upstream face of the next downstream wire the flow is turned and discharged through the slot between the wires.

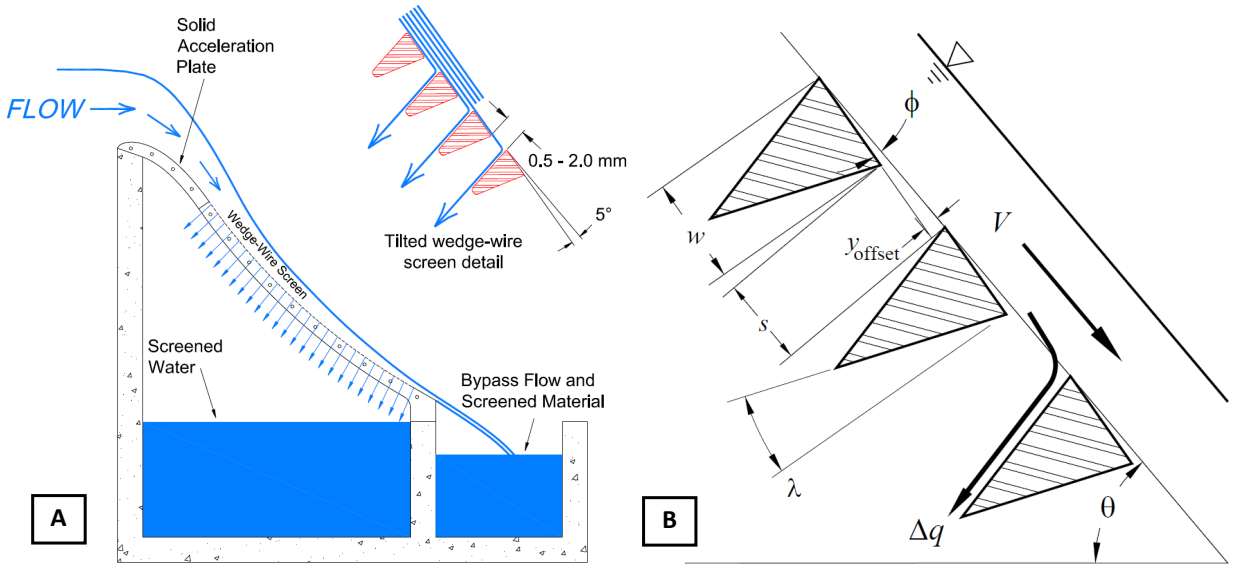

Fig. 1. (A) Features and typical arrangement of a Coanda-effect screen structure; (B) detail of screen geometry and key variables.

Previous Research

In a typical installation, flow conditions over the full length of a screen panel vary considerably. To enable the design of screen structures, Wahl (2001) tested three small screen material specimens in a fixed-slope flume inclined $\theta = 37°$ from horizontal to determine the variation of the screened flow as a function of screen geometric properties and flow conditions. Screens were installed at several distances down the flume slope and tested over a range of discharges. The tested screens all had slot widths (s) that were typical of prototype screens in the commercial products available at the time, either 0.5 mm or 1.0 mm. Screen capacity was related to the slot width, wire width (w), screen porosity $p = s/(s+w)$, wire tilt angle (ϕ), Froude number, Reynolds number, and Weber number.

The discharge through each screen slot was analyzed by considering the flow through the screen surface to be the combined result of the shearing action of the wire offsets and the orifice capacity of the slots due to the pressure head of the flow above the screen surface. The discharge equation was based on a virtual flow velocity vector representing the actual velocity parallel to the screen surface and a theoretical velocity component perpendicular to the screen surface computed as the pressure head of the flow converted into velocity head. The discharge equation included two coefficients, one related to the screen wire geometry and the Froude number of the flow (C_F) and the second determined experimentally to account for the influence of other factors (C_{cv}). Wahl (2001) related C_{cv} to the Froude number, $\mathsf{F} = V/(gD)^{0.5}$, Weber number, $\mathsf{W} = \rho V^2 s/\sigma$, and Reynolds number, $\mathsf{R} = Vs/\nu$, using the screen slot width (s) as the reference length in the latter two parameters. In these parameters V is the flow velocity across the screen, g is the acceleration due to gravity, D is the flow depth, ρ is the fluid density, σ is the surface tension constant of the fluid, and ν is the kinematic viscosity.

Subsequently, Wahl (2013) tested screens with wider slots (s = 2.0 mm) and wires having small relief angles, λ, mostly installed at slopes of $\theta = 15°$. Two of the screens previously tested by Wahl (2001) were also tested again. These studies used a new variable-slope flume, and one series of tests was conducted at a 30° incline to validate new equations relating discharge coefficients to flow parameters. Data collected during these tests were analyzed using the same discharge equation as used in Wahl (2001). In the new facility the range of tested Froude numbers was similar to that of Wahl (2001), but the range of Reynolds numbers was wider (both larger and smaller) and, due to the screens selected for testing, the range of Weber numbers was weighted toward smaller values. With these changes, the relationship developed in Wahl (2001) for predicting C_{cv} as a function of F, R, and W did not accurately match the observed coefficients in the new tests; deviations were as large as ±30%.

To address this deficiency, a new relation was developed relating C_{cv} to the angle of attack of the previously described virtual velocity vector approaching the screen slot. This was equivalent to relating the coefficient to the Froude number. Relations to the Reynolds and Weber numbers were inconsistent in this data set, so these factors were not included. Second-order polynomial equations related C_{cv} to the angle of attack, but a deficiency was that these relations could not be readily extended to much larger angles of attack, since they would predict increasing screen efficiency (inconsistent with the trend of the data) once the minima of the curves were reached. In addition, there were no experimental data available to develop relations that would apply to larger angles of attack. Typical prototype screen structures have low Froude numbers (and large angles of attack) at the upstream end of the screen, so it is important to understand this flow condition well to make good predictions of total screen performance.

To address this issue, an expanded series of tests was started in 2016 using the variable-slope test facility. Several of the previously tested screen specimens were evaluated over an even wider range of flow conditions, at slopes ranging from $\theta = 1°$ to 50°. Over this range neither of the previously developed relations could accurately predict the discharge coefficients of individual screens, much less multiple screens with varying properties. This made it necessary to develop a new discharge equation and a new relation to predict the discharge coefficient as a function of basic flow parameters. This paper describes the test facility and presents the new discharge equation, the accumulated test data from the several experimental campaigns, and the newly developed discharge coefficient relations.

EXPERIMENTAL PROGRAM

Test Facility

A unique 0.15-m (6-inch) wide adjustable-slope flume was constructed in the hydraulics laboratory of the Bureau of Reclamation to determine screen throughput under a range of hydraulic conditions. The facility is similar to the fixed-slope flume used by Wahl (2001), but with more flexibility to test a broad range of flow conditions. The facility was developed first for a project-specific study (Wahl 2013) and modified with a larger tailwater tank and improved flow measurement equipment for the most recent tests beginning in 2016. Fig. 2 shows the flume with its three screen test locations (top, middle, and bottom). Other views of the flume, head and tailwater tanks, and V-notch weirs are provided in supplemental Fig. S1. The maximum flow rate was 0.0076 m^3/s (0.27 ft^3/s). The head tank was nominally 0.61 m (2 ft) wide, 0.91 m (3 ft) long, and 0.61 m (2 ft) deep.

Fig. 2. Variable-slope screen testing flume. Additional views of the test facility are given in supplemental Fig. S1.

The objective was to determine the discharge capacity of screen slots located in the middle of a relatively long reach of prototype screen, but the first few slots of a tested screen are known to accept flow less efficiently (Wahl 2001). This occurs because the flow over the first slots is not aligned with the top surface of the screen wires and may also be affected by the boundary layer developed in the flume section leading to the screen. That boundary layer is gradually sheared off the bottom of the water column, so wires further downstream have a flow applied to them that has essentially no boundary layer (Wahl 2001). To make the testing represent mid-screen conditions, a divider plate was installed below the screens (Fig. 3) to separate the screened flow between an upstream reach (an adjustable distance of about one third to one half of the screen specimen length) and a downstream reach. The flow through the upstream section (waste flow) was collected, measured, and discarded, while the flow through the downstream slots was also collected and measured to provide the test result.

For the flow over the test portion of the screen, the depth, velocity, and dimensionless flow parameters were computed at the upstream and downstream ends of the test section to determine average values at the midpoint of the test section. Depths and velocities above the screen surface were not specifically measured, since previous measurements with a Pitot tube at the upstream and downstream edges of tested screens (Wahl 2001) showed that the velocities and depths could be reliably calculated knowing the discharge through the flume and the water level measured in

the head tank, applying a reasonable friction factor for the smooth-bottomed flume. The head tank water level was measured in a 100-mm-diameter (4-inch) stilling well equipped with a hook gage mounted on a vernier scale with 0.0003 m precision (0.001 ft). Discharges into the flume were measured with a 76-mm-diameter (3-inch) electromagnetic flow meter (Siemens SITRANS FM MAG 5100 W with SITRANS FM MAG 6000 controller, accuracy ±0.2% of flow rate), and the entrance to the top of the flume was calibrated during the testing to enable the inflow to also be determined from a head-discharge relationship (standard error = 3.7%). Flows through the upstream and downstream sections of the screen were collected in clear acrylic divider boxes (Fig. 3B) that allowed visual confirmation that there was no leakage between the two chambers, and flow rates were measured with custom 30° V-notch weirs calibrated in-place using time-volume measurements. Standard errors for the waste-flow and test-flow weirs were 5.8% and 4.0%, respectively.

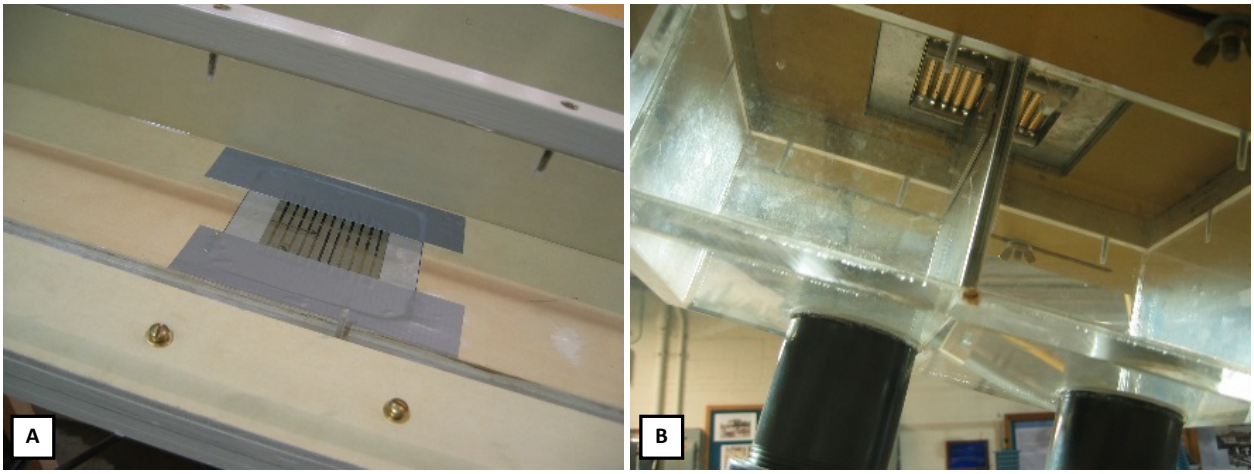

Fig. 3. (A) A screen installed in the test flume; (B) the transparent collection box beneath the flume.

Test Procedures

For each series of tests with a screen installed at one position in the flume, the flow was set first to the maximum pump discharge and then incrementally lower until there was little to no flow depth over the downstream toe of the screen. About 5 to 8 steady-state flow rates were typically tested for each screen configuration. For each run, the flow rate into the flume was determined either from the electromagnetic flow meter or the flume crest rating equation, and the flows through the waste and test sections of the screen were measured through the V-notch weirs. Weir box water levels were measured in stilling wells using hook gages with vernier scales with 0.0003 m (0.001 ft) precision. The flume slope for each test was determined with a digital level that recorded slope in degrees and percent with 0.1° / 0.1% precision. Slope measurements were made for both the right and left sides of the flume to verify similarity and the average slope value was recorded.

For each screen test position (top, middle, or bottom) the flow distance and elevation drop from the crest to the start of the screen was determined based on the flume slope and the geometry of the crest. Knowing the discharge into the flume, a flow profile was calculated from the crest (where critical depth was assumed) to the start of the screen. Friction losses were determined using the Colebrook-White equation to estimate friction factors, f, for the Darcy-Weisbach equation, using a rugosity of 0.00003 m (0.0001 ft) for the crest (a circular arc section of a PVC

pipe) and the flume (epoxy-coated marine plywood on the floor and left wall, and clear acrylic on the right wall). Values of *f* varied from about 0.018 to 0.025. To determine flow conditions at the downstream end of the waste section of the screen (and upstream end of the test section), a flow profile was calculated across the waste section for spatially varied flow with decreasing discharge (Chow 1959), with the average flow exiting through the screen at each slot determined from the measured flow through the associated V-notch weir. This screened flow was assumed to be evenly distributed among the waste slots. Similarly, a gradually varied flow profile was calculated over the test section of the screen to determine the flow conditions at the downstream end of the test section. Hydraulic parameters were calculated for the upstream and downstream ends of the test section (first and last tested slot), and average values at the midpoint of the test section were determined. These average values were used to develop correlations between the dimensionless flow parameters and the observed screened flow and calculated discharge coefficients. Flow depths over the tested portions of the screens were typically 3 cm (0.1 ft) or less, and velocities varied from about 0.9 to 4.0 m/s (2.9 to 13.1 ft/s).

A few screens with large wire tilt angles ($\phi > 6°$) exhibited skipping of the flow when tested at steep slopes at the bottom position in the flume. Skipping occurs when the Coanda effect (attachment of flow to the top surface of the wire) is lost so that flow detaches from the leading edge of a wire and skips over the wire and its downstream slot, producing a visible air void over the slot and reducing or eliminating discharge through the skipped slot. Cases of flow skipping were eliminated from the data sets analyzed here. Although flow skipping was associated with large wire tilt angles, steep slopes, high flow velocities, and shallow flow depths (i.e., large Froude numbers), no attempt was made in this study to develop criteria for defining thresholds for flow skipping. Supplemental Fig. S2 shows examples of normal and skipping flow.

Screens

Table 1 shows physical properties of tested screens, which represent screen configurations in common use at the time that the research program was started. The maximum nominal slot width for tested screens was 2 mm, but screens with slot widths up to 3 mm are now used on some hydropower intakes. All wire tilt angles were measured using an optical reflection method (Wahl 2001). Wire widths and slot widths were measured with calipers at several locations over the surface of each screen. The relief angles, λ, for each wire shape are the designated values given by screen manufacturers for each wire shape. Most of the reported dimensions match those given in previous works, but the wire tilt angles for screens A-5, A-8, B-1, and B-2 were adjusted slightly from the values reported in Wahl (2013) based on new measurements. Screens #1 and A-5 were tested most extensively. Screen #1 was tested at 10 different combinations of flume slope and test position in the flume, with a total of 118 different runs. The other screens were each tested at about 4 to 6 different slopes and/or positions with about 20 to 60 individual runs. All screens were in new condition at the time of testing; wear of the leading edges of wires in heavily sediment-laden flows is recognized to cause a loss of screen capacity over time (Wahl 2003).

A custom mounting block was constructed for each screen to allow it to be mounted flush with the flume surface. Divider plates separated the upstream waste section of the screen and the downstream test section. The divider plates fit tight beneath the screen surface and the support bars, and modeling clay was used to further ensure a watertight seal between the two sections during testing. Fig. 4 shows one of the tested screens installed into its mounting block.

Table 1. Properties of tested screens. Positions tested indicates the number of unique combinations of screen slope and position within the test flume (top, middle, or bottom location).

Screen	Relief angle λ (degrees)	Wire tilt angle ϕ (degrees)	Avg. slot width s (mm)	Avg. wire thickness w (mm)	Offset height y_{offset} (mm)	Specimen width (mm)	Specimen length (mm)	Specimen length (slots)	Support bar spacing (mm)	Support bars —	Number of flow tests —	Positions tested —
A-1	10	3.3	1.987	4.759	0.382	98	98	14	84	9.5-mm ◯	45	5
A-2	10	6.5	2.007	4.712	0.757	76	79	11	54	9.5-mm ◯	23	4
A-3	10	6.5	2.010	4.707	0.757	76	79	11	54	9.5-mm ◯	25	4
A-4	10	6.3	2.013	4.713	0.729	76	79	11	54	9.5-mm ◯	27	4
A-5	10	5.3	1.985	4.717	0.652	76	79	11	54	9.5-mm ◯	62	9
A-6	10	7.5	1.928	4.705	0.861	76	79	11	54	9.5-mm ◯	24	4
A-7	10	6.3	2.010	4.750	0.733	76	79	11	54	9.5-mm ◯	46	5
A-8	10	6.0	1.957	4.738	0.800	76	79	11	54	9.5-mm ◯	104	4
B-1	13	5.5	2.046	4.604	0.498	89	89	13	51	6.4-mm □	28	5
B-2	13	5.8	2.053	4.624	0.753	89	89	13	52	6.4-mm □	22	5
#1	17.5	3.8	1.021	2.390	0.227	93	76	22	70	9.5-mm ◯	118	9
#2	12.5	3.6	0.993	1.549	0.158	104	72	40	19	4.0-mm ◯	26	4
#3	11	6.9	0.467	1.496	0.234	87	73	36	13.5	4.0-mm ◯	38	6

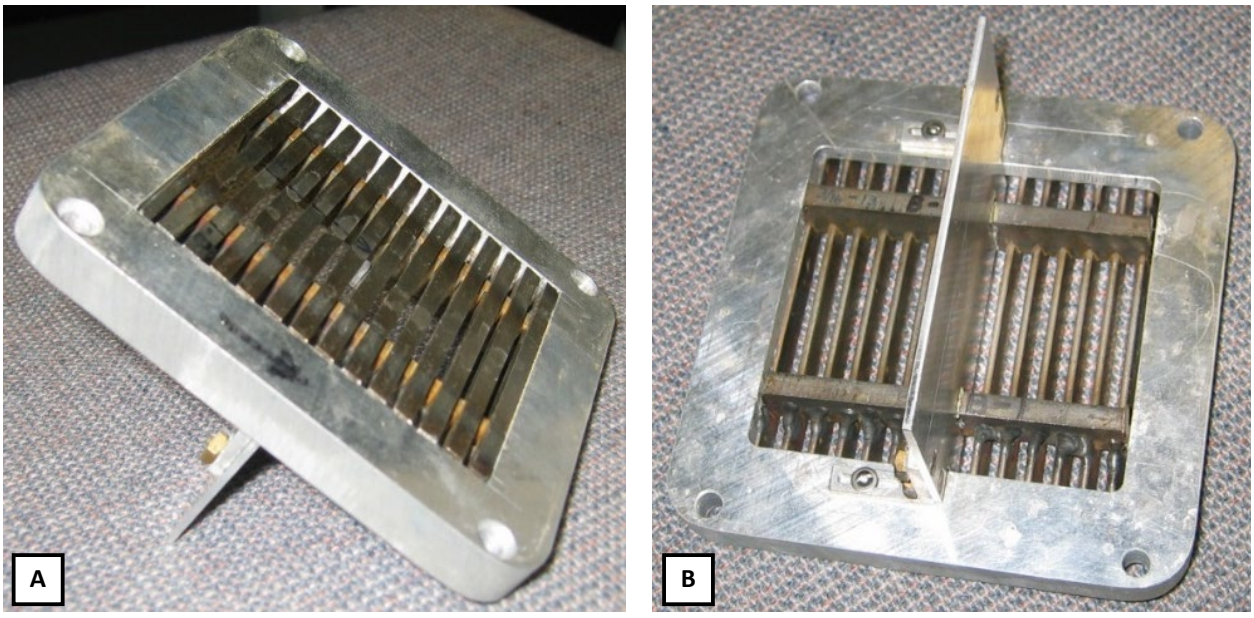

Fig. 4. (A) Test screen B-1 in mounting block; (B) a view of the underside of the screen with divider plate installed. Flow direction is left to right for both photos.

Initial Testing: Influence of Screen and Flume Width

A series of tests was run to confirm again (as observed by Wahl 2001) that results were independent of the ratio of flume width to screen width. The flume was constructed wider than the screens because the screens available for testing had a variety of widths, and it was impractical to make screens span the full width (or more) of the flume while still being easily interchangeable. Also, there was concern that a very narrow flume would cause wall effects to distort the results. Test runs at 5° and 26° slopes were made with different widths of screen open to the flow by masking off portions of the screen width with tape, thus varying the ratio of flume to screen width in the range of 2.3 to 4.6. No difference in screened flow was observed as a function of the width ratio. However, this testing was unable to evaluate width ratios in the range of 2.3 down to 1.0.

Computer Modeling

In addition to the physical experiments, width ratio effects were studied with computational fluid dynamics (CFD) modeling (Dzafo 2019). The steady-state flows through one screen specimen (screen A-5) were simulated using the ANSYS Fluent finite volume code to solve the Reynolds-averaged continuity and Navier-Stokes equations with a standard k-ε turbulence model. CFD models were run for 3D cases having ratios of flume width to screen width greater than 1.0 and for 2D cases in which the screen and flume width were effectively equal. A rendered view of the flume and the screen specimen is shown in Fig. 5. The computational domain included the screen, the full 152 mm (6.00 in.) width of the flume, and a 460 mm (1.5 ft) length of the flume approaching the lower screen test location of the test facility. Boundary conditions consisted of an upstream mean velocity matching experimental conditions, a hydrostatic pressure distribution in the flow exiting the downstream end of the flume and the bottom of the screen, atmospheric pressure above the water surface and in the collection box beneath the screen, and impermeable surfaces forming the sides and floor of the flume. Free surface flow was simulated using the volume of fluid (VOF) method. Reasonable values for turbulence intensity (5%) and the

turbulent viscosity ratio (eddy viscosity / dynamic viscosity = 10) were assumed at the inlet boundary.

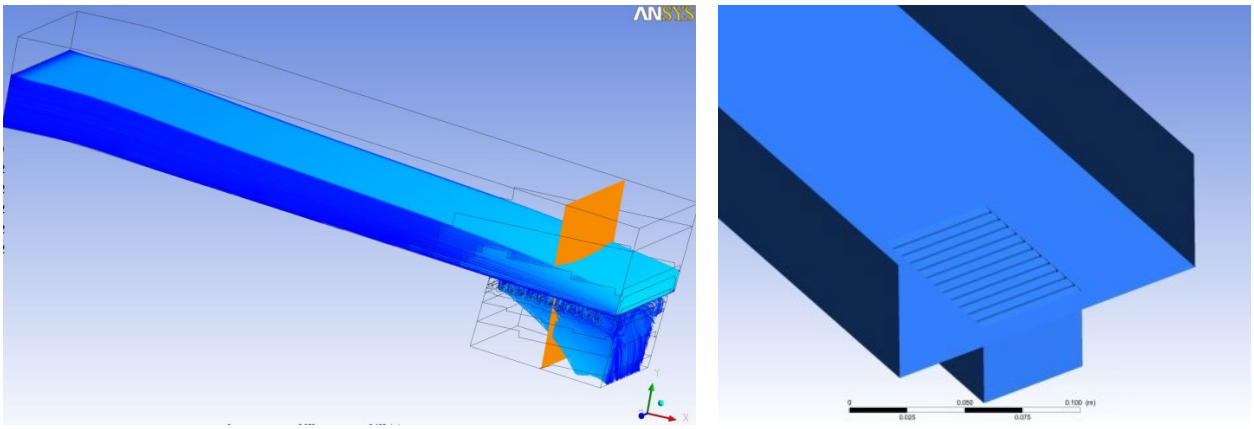

Fig. 5. Rendered views of the geometry used in the numerical simulations.

Early phases of modeling used triangular and tetrahedral cells for 2D and 3D cases, but final simulations used quadrilateral (2D) and hexahedral cells (3D). This produced more stable results that were less sensitive to the degree of mesh refinement. To improve the efficiency and accuracy, the mesh was made coarsest in the flume reach approaching the screens where the flow is accelerating smoothly under the action of gravitational forces, gradually finer over the screen surface, and finest in the vicinity of the screen wires and slots. Considering the flow physics, an enhanced wall treatment modeling strategy was adopted near the screens (Gharbi et al. 2009), with a fine mesh that placed the first node at about $y+ = 1.0$, where $y+ = yu_*/\nu$ and y is the distance from the boundary, u_* is the shear velocity, and ν is the kinematic viscosity. This approach resolves velocity details close to the screen surface where velocity gradients are large and openings between screen wires are small. Examples of 2D and 3D meshes are shown in supplemental Figs. S3-S5. The final computational domain ranged from 0.12 to 0.22 million cells for 2D simulations, and 1.3 to 2.2 million cells for 3D simulations.

Laboratory results were used to validate the numerical modeling. For assessing the accuracy of numerical results, *Relative Average Error (RAE)* values were calculated, $RAE = |q_{exp} - q_{CFD}|/q_{exp}$, where q_{exp} is the experimental discharge per unit width through the test section of the screen (downstream from the divider plate), and q_{CFD} is the numerically simulated unit discharge through the test section. CFD simulations were used to study flume to screen width ratios ranging from 1.75 to 1.0 (a 2D case), as shown in Table 2.

The steady state solution was obtained after initial test calculations where several different under-relaxation factors were used for the momentum equation. The residuals were used to monitor the iterative convergence using different mesh sizes. The PRESTO! (PREssure STaggering Option) pressure discretization scheme exhibited the best convergence on this simulation. Convergence was reached when the normalized residuals of each variable were below 0.0001. After the first convergence of the numerical solution the mesh was refined, and the model was run again until consistent results were obtained at higher mesh densities.

Table 2. Flume to screen width ratios studied using CFD. Flow conditions at start of screen match specific physical experiments in the laboratory.

Parameter	Case 1	Case 2	Case 3	Case 4
flume to screen width ratio	1.75	1.5	1.25	1.0
flume width / screen width, mm	152.4 / 86.8	152.4/101.6	152.4/121.9	152.4/152.4
flume and screen slope, θ	5.3°	5.3°	26.3°	26.3°
inflow unit discharge, $m^3/s/m$	0.0458	0.0374	0.0447	0.0327
velocity at start of screen, m/s	1.70	1.22	3.00	2.84
depth at start of screen, m	0.0270	0.0306	0.0149	0.0115

Fig. 6 shows the distribution of flow through screen slots for a typical case. The results confirm that the upstream part of the screen (especially the first slot) accepts less flow, consistent with the previous description of how the flow develops and gradually aligns to the angle of the tilted wires. Once the flow is developed, the flow rates through downstream slots are relatively uniform.

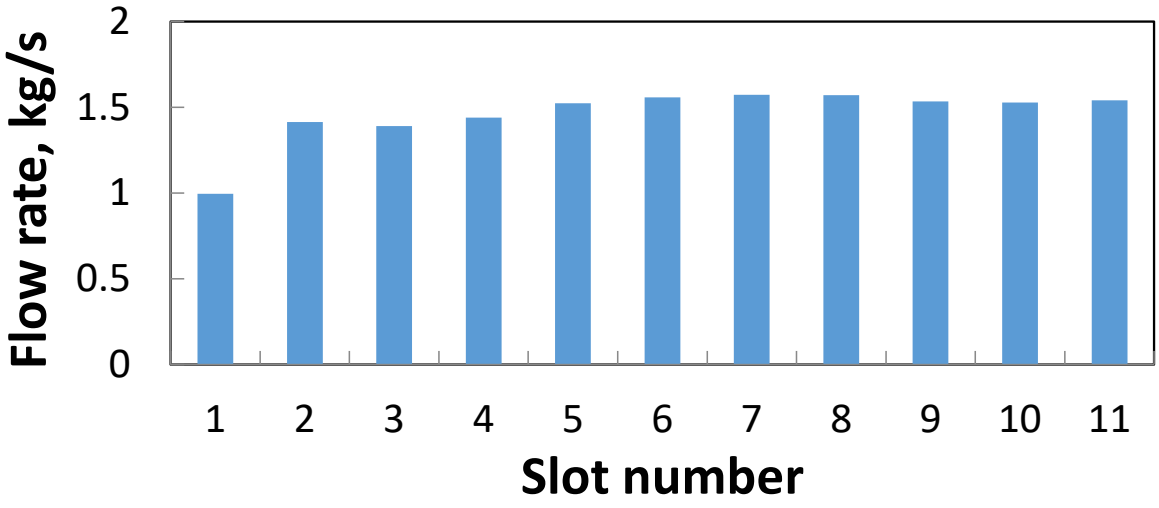

Fig. 6. Typical CFD-simulated flow rates through individual screen slots. Slot number 1 is furthest upstream.

Table 3 shows relative average errors for 2D CFD runs (flume to screen width ratio = 1) vs. laboratory experiments and for 3D CFD runs (flume to screen width ratio > 1) vs. laboratory experiments. In general, both types of CFD simulations predicted smaller flows than those obtained in the lab experiments. The average difference between 2D CFD and experimental results was about -4.5% for flume slopes of 5° and 26°. For the 3D CFD models, differences were -2.6% for the 26° flume slope and -4.3% for the 5° flume slope. These small differences between CFD results and experimental data indicate that the CFD models reasonably represent the flow situation, and the similarity of the 2D and 3D results confirms that edge effects are minor.

Table 3. Relative average errors (RAE) from comparison of experimental and numerical values of discharge screened per unit area for simulations of screen A-5.

Flume slope	RAE *(%) 2D model*	RAE *(%) 3D model*
5°	2.84 - 6.26	3.48 - 5.07
26°	3.28 - 5.56	1.71 - 3.57

VARIABLE-SLOPE TESTING AND NEW DISCHARGE EQUATION

The screens shown in Table 1 were tested at top, bottom, and middle positions in the flume at a variety of slopes ranging 1° to 50°. Testing in 2016 and 2017 included a full range of slopes, especially very flat and very steep slopes, and mostly used the top and bottom screen positions. Tests performed in 2012 at slopes of 15° and 30° at all three screen positions were also included in the data analysis. Slopes up to 60° are common in field installations, but physical limits of the apparatus made it logistically difficult to test at slopes steeper than 50°.

Initial analysis of the collected data was attempted with the same discharge equation used in Wahl (2001) and Wahl (2013), and the observed discharge coefficients were compared to those predicted by the functions developed in those studies. Unfortunately, across the wide range of test conditions there was poor agreement of the observed and predicted coefficients, with errors up to ±35% for one of the tested screens (Fig. 7). Considering multiple screens, ratios of predicted to observed discharge coefficients ranged from about 0.55 to 1.6.

Ultimately, no suitable relation was found between the discharge coefficients computed by the previous methods and the dimensionless flow parameters (F, R, and W), and it became necessary to develop a new discharge equation. The new equation is based on the screen geometry and flow situation illustrated previously in Fig. 1B. The tilted-wire construction causes the screens to shear a thin layer of water from the bottom of the water column. If the flow velocity across the screen face is V and is presumed to remain constant as the flow is turned, the unit discharge through the screen at each wire is simply

$$\Delta q = V \cdot y_{\text{offset}} \tag{1}$$

where y_{offset} is the thickness of the water layer sheared off by the raised offset. This equation assumes several idealized conditions:

- The flow across the screen is attached to and parallel to the upper surface of each wire and cleanly detaches from the downstream edge of each wire without any change of flow direction so that it proceeds straight into the face of the next downstream wire (no gravitational deflection of the jet), where it is turned with 100% efficiency through the screen.
- The velocity profile is uniform (no significant boundary layer) and is represented by the depth-averaged velocity of the flow over the screen, V.
- The thickness of the diverted flow stream is equal to $y_{\text{offset}} = (s + w \cos \phi)\sin \phi$, or for small values of ϕ ($\leq 9°$), $y_{\text{offset}} = (s + w)\phi$, where s and w are the slot width and wire width, respectively, and ϕ is expressed in radians.

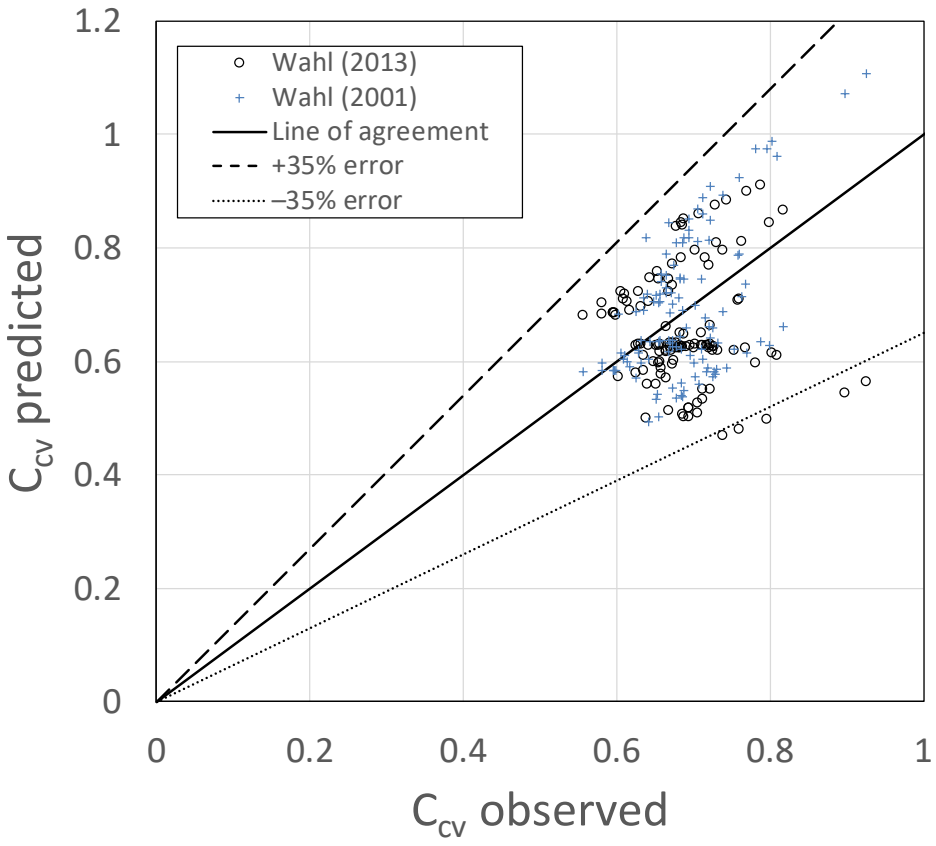

Fig. 7. Predicted and observed screen discharge coefficients for screen #1 with previously developed models.

A discharge coefficient C_{offset} is introduced to account for deviations from these assumptions:

$$\Delta q = C_{\text{offset}} \cdot V \cdot y_{\text{offset}} \tag{2}$$

In particular, it is expected that as flow depth above the screen increases, hydrostatic pressure against the screen surface may cause the thickness of the water layer sheared away by each wire to exceed the offset height and approach the slot width, s. Discharge coefficients greater than 1.0 should be expected in this case.

DATA ANALYSIS

Using Eq. 2, values of C_{offset} were determined from the experiments and relations were explored to the Froude number and several forms of the Reynolds and Weber numbers. The Froude number was calculated with the slope adjustment presented by Chow (1959):

$$\mathrm{F} = \frac{V}{\sqrt{gD\cos\theta}} \tag{3}$$

Reynolds and Weber numbers were computed using the depth-averaged mean velocity across the screen as the velocity reference and with several different length references, including the flow depth, slot width, wire width, and offset height (y_{offset}). The best correlations were obtained

using the slot width to compute the Reynolds number and the offset height (the nominal thickness of the sheared water layer) to compute the Weber number:

$$\mathsf{R} = \mathsf{R}_{\text{slot}} = \frac{Vs}{\nu} \tag{4}$$

$$\mathsf{W} = \mathsf{W}_{\text{offset}} = \frac{\rho V^2 y_{\text{offset}}}{\sigma} \tag{5}$$

Fig. 8 shows relations between C_{offset} and F, R, and W. For clarity, the charts only show data from screen #1, but trends for other screens were similar. Strong inverse relations to each parameter are apparent, with C_{offset} generally increasing as the values of F, R, and W decrease. The largest C_{offset} values occur for flatter flume slopes and low flow velocities (i.e., screens installed at the upper test positions). C_{offset} reduces asymptotically toward a constant value for large values of F, R, and W.

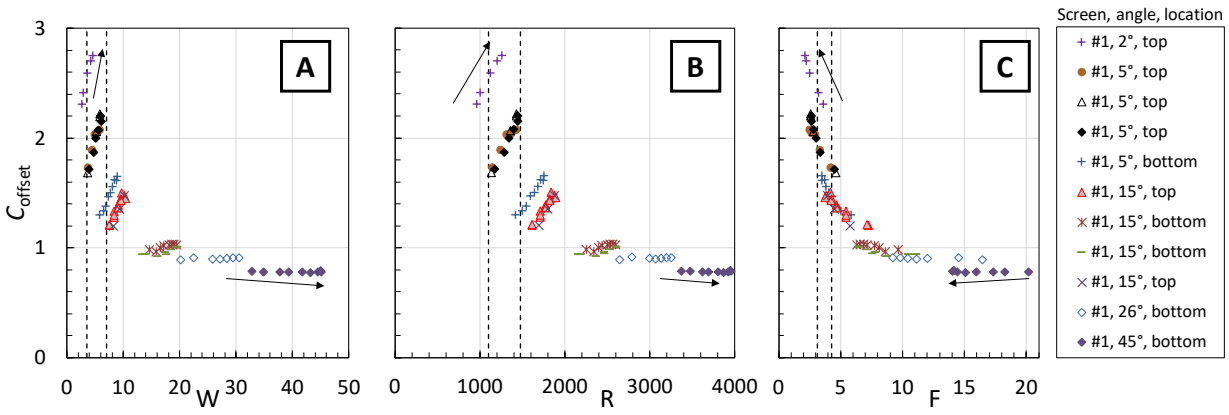

Fig. 8. Relations between C_{offset} and (A) Weber number, (B) Reynolds number, and (C) Froude number for screen #1. Arrows indicate direction of increasing flow for tests performed at fixed slopes.

The question of which flow parameter has the dominant influence on the discharge coefficient is not easily answered from these data. Because all three parameters varied simultaneously during the tests, the influence of each cannot be isolated. After carefully reviewing the data it was suspected that some of the correlations were spurious, since F, R, and W all increase in proportion to a power of the flow velocity.

When the data were examined closely, the relation with W looked particularly promising because subsets of test values in different flow rate bands (e.g., highest-flow tests, lowest-flow tests, etc.) appeared to define a family of approximately parallel power curves. This suggests that C_{offset} might be represented as a power curve function of W, with the multiplier or exponent modified by R and/or F.

To investigate spurious correlations, data were filtered to isolate variation of each parameter. Fig. 9 shows data from screen #1 over a wide range of F but within only the narrow bands (nearly constant values) of W and R indicated by the dashed lines in Figs. 8A and 8B. Again, for clarity, only data from screen #1 are shown, but similar behavior was observed in data from other tested screens. The inverse relation between C_{offset} and F is readily visible. Fig. 10 shows slices of data spanning wide ranges of R and W, limited to the narrow band of F indicated in

Fig. 8C, and inverse relations are again apparent. Unfortunately, for any single screen it was impossible to hold a constant value of R while varying W or vice versa, so one cannot determine whether Fig. 10 demonstrates distinct R and W effects, or similar effects that are spuriously correlated.

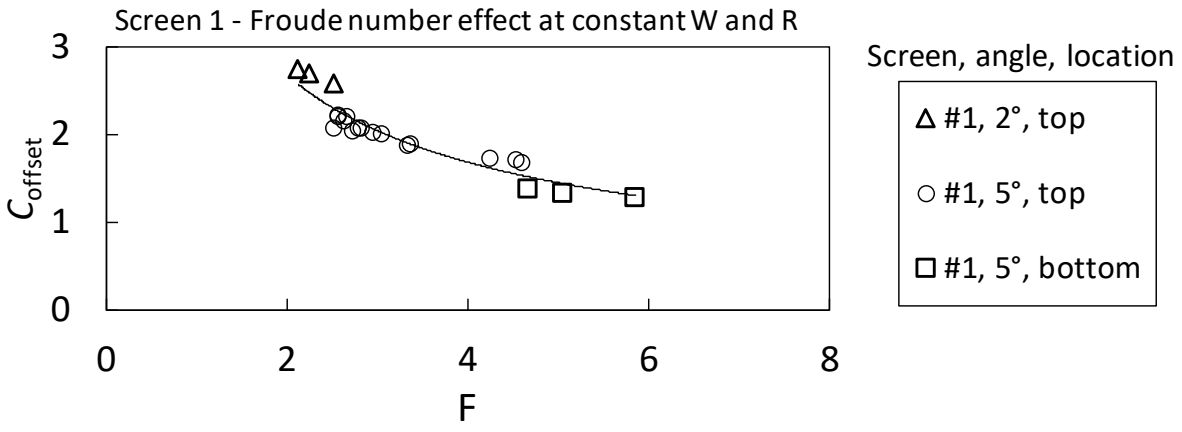

Fig. 9. The Froude number effect is illustrated by filtering data from screen #1 to show C_{offset} values vs. F at nearly constant W and R. The range of W is 3.5 to 7, corresponding to the vertical slice in Fig. 8A.

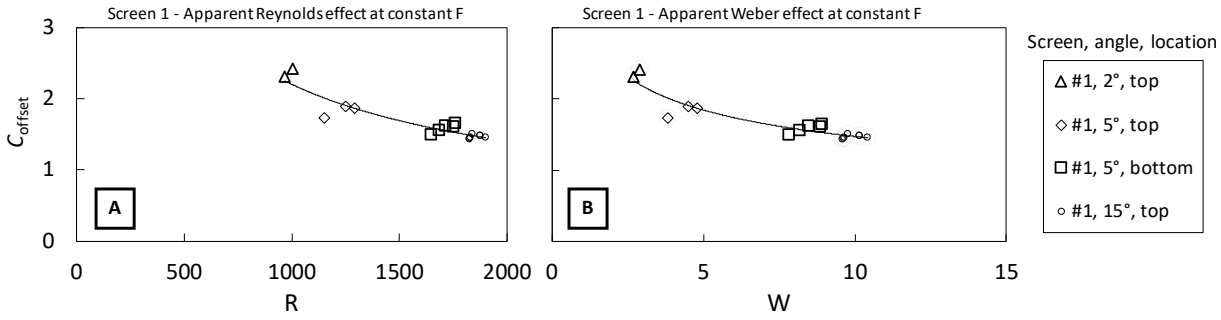

Fig. 10. Apparent effects of Reynolds number (A) and Weber number (B) are illustrated by filtering data from screen #1 to show values at nearly constant Froude numbers (3.1 to 4.3) within the vertical slice indicated in Fig. 8C.

Variable-Temperature Tests

To isolate the effects of R and W, a series of tests of screen #1 were performed while the water was gradually chilled from 21°C (70°F) to 3°C (37°F) at a constant discharge and fixed flume slope. Water viscosity increases about 60% over this temperature range, but the surface tension coefficient increases by only about 3%, so this provides a way to observe Reynolds number effects almost independent from Weber number effects. Additionally, testing was repeated at three different flume slopes and discharges to obtain a set of data points with variable Weber numbers and nearly constant Reynolds numbers. The Froude number for the full set of variable-temperature tests was nearly constant ($5.0 < F < 5.2$).

Fig. 11 shows a definite relation to W, while Fig. 12 shows no relation to R in three data sets restricted to narrow ranges of W. The data collected at one slope setting ($\theta = 14.6°$) suggested a

slight trend with R, but there was no trend when the data from all three slopes were combined and normalized to eliminate the variation due to W.

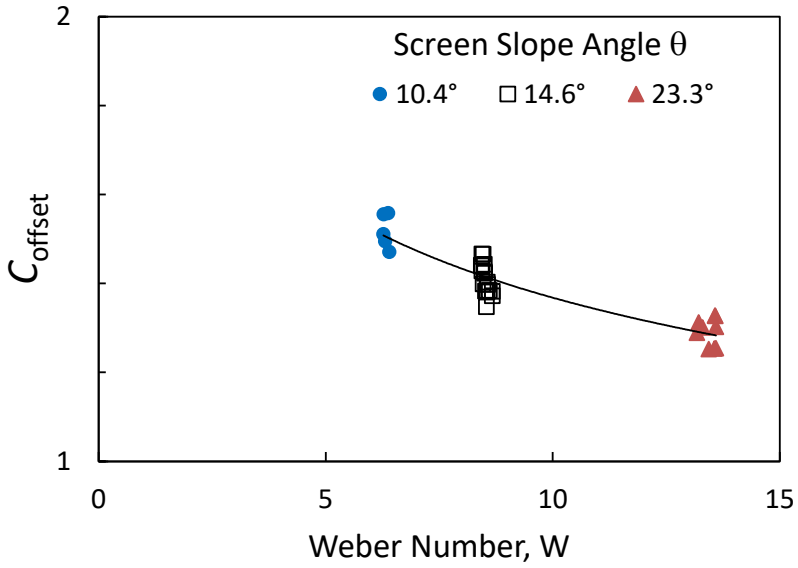

Fig. 11. The Weber number (surface tension) effect is clearly demonstrated in tests run with nearly constant Froude numbers (4.74 to 5.08) at three different Weber numbers. A similar trend is seen in Fig. 10B for a lower range of Froude numbers.

Discharge Coefficients related to W and F

To enable prediction of discharge coefficients, relations between C_{offset} and basic flow and screen properties were investigated. Fig. 8 showed that C_{offset} was inversely related to both W and F. Power curves and exponential functions of each were considered, and a power curve of W most effectively collapsed the data of multiple screens toward a single relationship (Fig. 13). Best-fit equations minimizing the sum of the squared relative errors in the predicted values of the discharge coefficients were determined for data sets collected from single screens and for combined data sets comprising multiple screens. Successful curve fits were obtained initially with equations of the form:

$$C_{offset} = (a + b\Phi)(W)^c \tag{6}$$

with a, b, and c being curve-fitted numerical constants, and $\Phi = F^2/(2+F^2)$. Equations utilizing F at the heart of the power curve equation (rather than W) fit poorly. Equations based on Weber numbers defined using the slot width and wire width were effective for single screens (where the geometry of the screen was fixed), but less effective when applied to multiple screens with different wire and slot dimensions. The Φ parameter was more effective than F in the multiplier term of Eq. 6. Wahl (2001) showed that this ratio is the kinetic energy fraction of the flow specific energy, while its complement $2/(2+F^2)$ is the fraction of the specific energy associated with flow depth. Functions of F and other variables were also considered for the exponent on W (in place of c) but were rejected due to inconsistent results. Some equation forms with additional parameters and complexity provided slightly better regression results, but the simpler form of Eq. 6 was preferred.

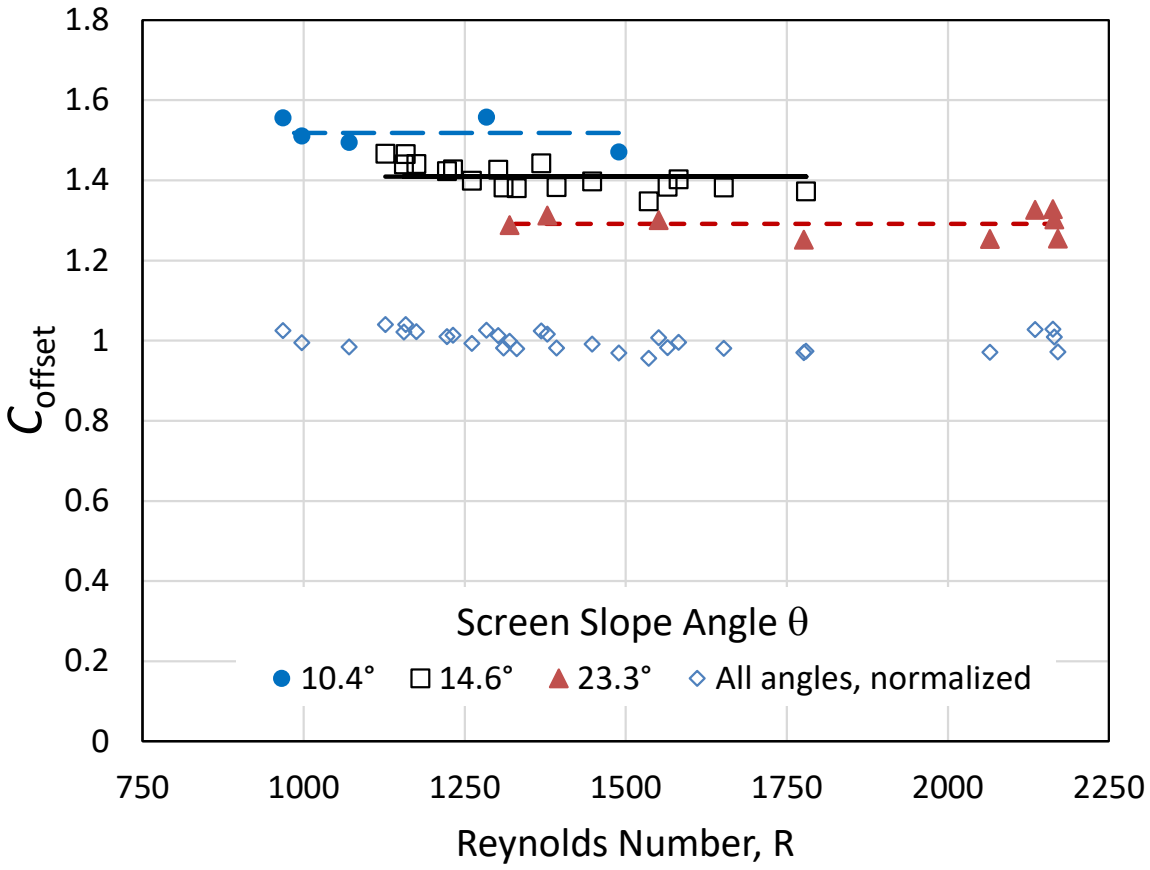

Fig. 12. Variable temperature tests show that there is no Reynolds number effect on the discharge coefficient. All data sets shown here have the same Froude number, and each data set at a given slope has a different, fixed Weber number. The combined data set is normalized about each of the respective averages to remove the Weber number effect.

After fitted values of a, b, and c were determined for individual screens, a strong linear relation was found between a and b, and a plot of a vs. b revealed three data clusters (Fig. 14). The largest cluster comprised 10 screens (#3 and all A- and B-series screens except A-1). The linear relation between a and b was substituted into Eq. 6, and this produced an equation for predicting C_{offset} using only two fitted parameters:

$$C_{offset} = [a + (1.077 - 0.970a)\Phi]\cdot \mathrm{W}^{c} \quad (7)$$

Table 4 shows results of fitting Eq. 7 to individual screens and the cluster of 10 screens with similar a values. RMS errors ranged from about 1.5% to 7% for individual screens and were just under 8% for the group of 10 screens. The fitted values of the exponent c varied from -0.09 to -0.22 with an average of -0.14, but there was no discernible pattern in its value. No measurable property of the screens could be identified to explain why screens #1, #2, and A-1 had significantly different fitted values of a, but some intangible factors were noted. Screen A-1 had a polished appearance that was different from the other A-series screens and seemed to have an enhanced sharpness of the wire edges that could not be readily quantified but may have affected its performance. Another possibility is metallurgical differences that may have given

some screens varying degrees of hydrophobicity; the tested screens were obtained from various sources over a period of years and although all are stainless steel, the exact alloys are unknown.

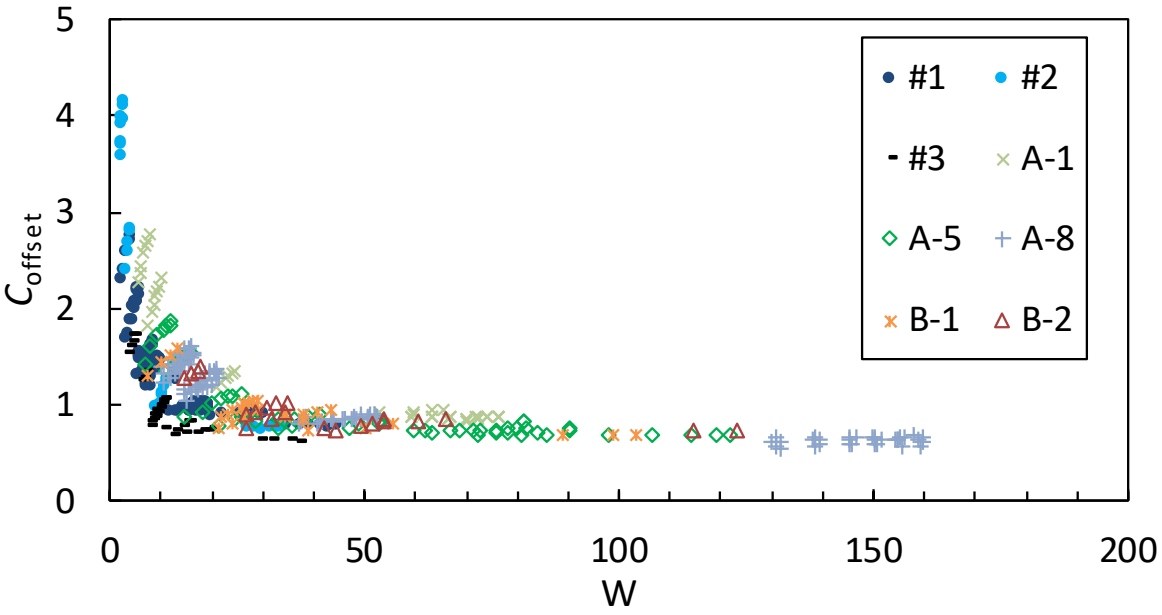

Fig. 13. C_{offset} vs. W data for multiple screens.

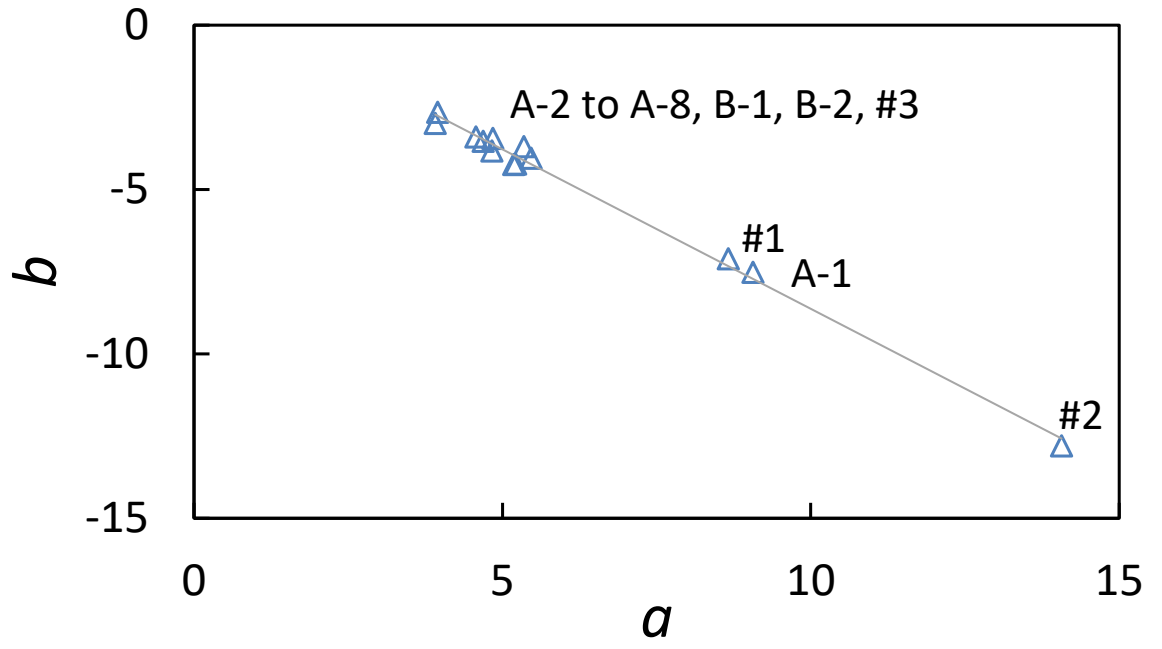

Fig. 14. Linear relation between curve-fit parameters *a* and *b* of Eq. 6. Best-fit linear regression line is $b = 1.077 - 0.970a$.

Table 4. Coefficients of Eq. 7 and curve-fitting results.

Screen	*a*	*c*	RMS error, %	Number of tests
#1	8.68	-0.158	4.35	118
#2	14.26	-0.215	3.06	26
#3	5.30	-0.212	3.74	38
A-1	8.89	-0.106	2.06	45
A-2	5.07	-0.154	3.21	23
A-3	4.60	-0.125	1.64	25
A-4	5.31	-0.151	1.94	27
A-5	5.43	-0.134	6.33	62
A-6	3.88	-0.087	1.94	24
A-7*	5.19	-0.148	2.70	42
A-8	4.81	-0.134	4.47	104
B-1	4.73	-0.130	6.07	28
B-2	4.24	-0.118	6.73	22
#3, A-2, A-3, A-4, A-5, A-6, A-7, A-8, B-1, and B-2	4.86	-0.138	7.78	396

* To avoid effects of flow skipping, analysis of screen A-7 was limited to tests with $W < 135$

The flow skipping described previously was avoided in the tests when it was readily visible (no discharge data collected), but screen A-7 exhibited a gradual reduction of C_{offset} at $W > 140$ (supplemental Fig. S6), and even though skipping was not noted visually during the tests, the relatively steep 6.3° tilt of the wires for this screen makes it probable that skipping was responsible for the reduction of discharge. Screen A-6 exhibited obvious flow skipping from one out-of-plane wire when the Weber number exceeded 130 during tests at a slope of 17°. Flow testing was not performed on A-6 once skipping began, so the reduction of flow was not quantified. Experience with these two screens suggests that a Weber number $W > 130$ might be a trigger for the onset of flow skipping, but screen A-8 (with 6.0° wire tilt) exhibited no significant reductions of discharge at Weber numbers as high as $W = 160$. Flow skipping could be related to a combination of several factors, including values of W, F, and the wire tilt angle, ϕ. Additional testing is needed to determine general performance limits.

The observation that screens have individual performance characteristics suggests that laboratory testing should be performed whenever the most accurate predictions of screen discharge are needed. However, 10 of the 13 screens tested here performed similarly enough that they can be reasonably modeled by Eq. 7 using the set of coefficients provided in the last row of Table 4. When testing cannot be performed on a specific screen, these coefficients can be adopted as default values to be used until specific tests can be made.

Fig. 15 demonstrates the fit of Eq. 7 to the observed discharge coefficients for screen #1. Observed values from each test are overlaid by lines indicating predicted values and the equation explains most of the variation of the observed values. Fig. 16 shows the predicted vs. observed discharge coefficients for screen #1 and a comparison back to Fig. 7 shows the dramatic improvement obtained with the new model. The RMS error of discharge coefficients for screen #1 is 4.35%.

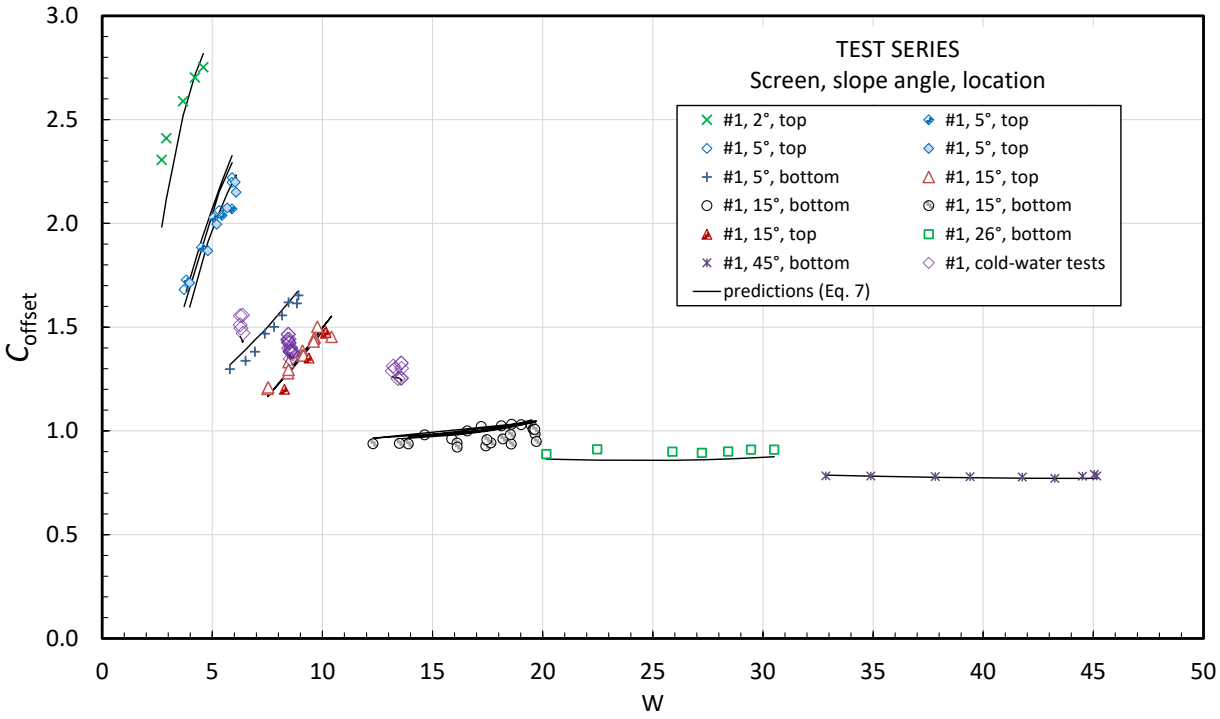

Fig. 15. C_{offset} values from screen #1 testing compared to Eq. 7 predictions.

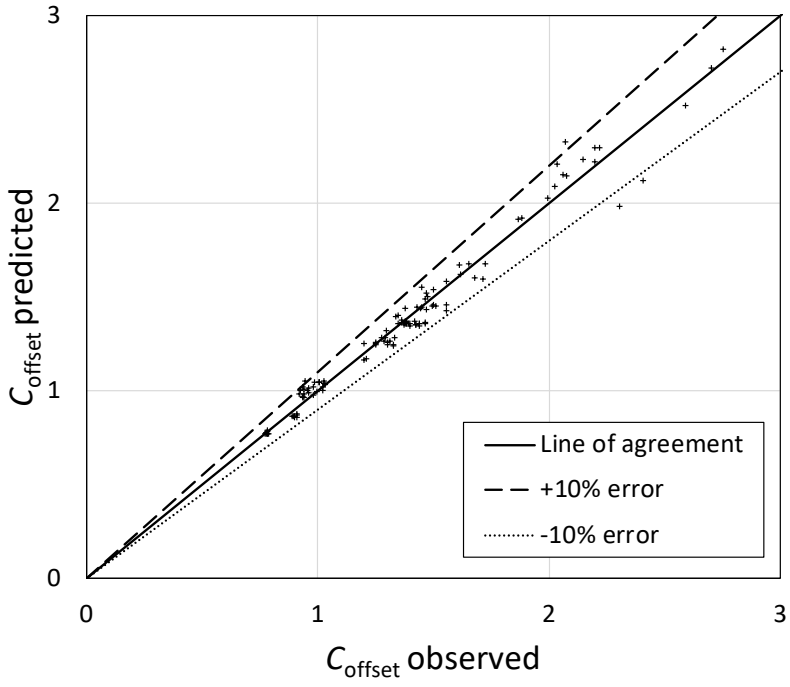

Fig. 16. Predicted and observed discharge coefficients for screen #1 showing dramatic improvement from Fig. 7. Average error is -0.32%. RMS error is 4.35%.

CONCLUSIONS

A unique, variable-slope test flume was used to measure the screening capacity of 13 different Coanda-effect screens having a range of wire thicknesses, slot sizes, and wire tilt angles. Tests were conducted at slopes ranging from 1° to 50°. A new discharge equation was developed, and discharge coefficients were inversely related to the Froude number (F), Reynolds number (R), and Weber number (W), but the latter two effects could not be isolated in initial tests. Testing at water temperatures from 3°C to 21°C (37°F to 70°F) was used to independently vary the viscosity, and the results showed that surface tension strongly affects discharge, but viscosity has no effect. Using this improved knowledge of the flow physics, discharge coefficients were related to a power function of W modified by factors related to F. This relation was significantly more accurate than previously developed equations (uncertainty reduced by a factor of about 3).

To some degree each screen exhibited a unique discharge coefficient relation, even though the slot widths, wire widths, and wire tilt angles of each screen were accounted for in the discharge equation. However, 10 of the 13 screens could be modeled reasonably by a single discharge coefficient relation that is suggested for default use in the absence of screen-specific tests.

Screen discharge coefficients are most dependent on W and F at low values of each parameter, which occur when velocities are low, depths are large, and the screen slope is small. Screen performance was most closely related to W computed with the offset height of the tilted wire serving as the reference length, so low W values and high dependence on surface tension occur when the wire tilt angle is small. At large W and F, discharge coefficients approach a constant value, but drop if or when flow skipping takes place (water separating from the leading edge of wires and jumping over subsequent screen slots); skipping at large W and F values affected two of the tested screens, but relating the onset of skipping to specific critical values of W, F, ϕ, or other factors was outside the scope of this study.

The performance of a complete screen structure depends on the variation of screen discharge coefficients over the length of the screen. To analyze prototype structures, the relations developed here have been incorporated into an existing spatially varied flow model of a complete screen structure, described in Wahl (2001), and the updated computer program is available from the lead author. Although the testing described here considered only planar screens, the computer program also accounts for screen curvature like that shown in Fig. 1.

Three areas for continued research and development are suggested:

- Flow skipping (loss of the Coanda effect) can be a practical problem when screens have large wire tilt angles or are installed on steep slopes or in structures with large drop heights. Testing is needed to develop reliable criteria for avoiding this condition.
- Although Coanda-effect screens are hydraulically self-cleaning, the self-cleaning action is not always sufficient to prevent some types of debris from clinging to the screen surface and building up to a point that restricts flow. Research is needed to enable predicting the loss of self-cleaning action. Future research could also explore methods to improve self-cleaning.
- Aerated flow in the receiving chamber beneath a Coanda-effect screen is a potential problem that can cause bulked water levels to become high enough to exert backpressure beneath the screen surface, which may reduce discharge capacity or lift screen panels out

of place if not firmly secured. Studies to quantify flow bulking could help avoid such performance issues.

DATA AVAILABILITY STATEMENT

All data, models, and code that support the findings of this study are available from the corresponding author upon reasonable request.

ACKNOWLEDGMENTS

This work was funded by the Bureau of Reclamation Research Office, Science & Technology Program. Student intern Dallas McKeough assisted with the collection of experimental data during 2016. Bryan Heiner provided internal peer review of this paper and was instrumental with model maker Marty Poos in configuring the flow chiller that enabled the cold-water testing. Machinist Dane Cheek constructed many of the unique test facility components. The screen test facility was originally constructed for work funded by Coanda Water Intakes, Ltd., Kamloops, BC, Canada.

NOTATION

The following symbols are used in this paper:

a = curve-fitted parameter
b = curve-fitted parameter
C_{cv} = combined contraction and velocity coefficient
C_F = coefficient related to alignment of approach flow with screen opening; a function of the Froude number
C_{offset} = discharge coefficient for discharge equation based on offset height
c = curve-fitted parameter
D = flow depth
F = Froude number
f = friction factor for Darcy-Weisbach friction loss calculations
g = acceleration due to gravity
p = screen porosity, $s/(s+w)$
R = Reynolds number
s = open slot width between wires
u_* = shear velocity
V = velocity tangent to screen surface
W = Weber number
w = screen wire width
y = distance from boundary
$y+$ = nondimensional distance from boundary, $(u_*)y/\nu$
y_{offset} = offset height created by tilted wire
Δq = unit discharge through one screen slot
θ = slope angle of the screen surface, measured from horizontal
λ = wire relief angle
ν = kinematic viscosity
ρ = fluid density
σ = surface tension force per unit length

Φ = kinetic energy fraction of the flow specific energy, $F^2 / (2 + F^2)$
ϕ = wire tilt angle

SUPPLEMENTAL DATA

Figs. S1-S6 and video S1 showing details of the test facility, CFD computational meshes, and the flow skipping behavior are available online in the ASCE Library (ascelibrary.org). Video S1 is also available at: https://www.usbr.gov/tsc/techreferences/hydraulics_lab/pubs/PAP/PAP-1193_video_S1.mp4

REFERENCES

Chow, V. T. 1959. *Open-Channel Hydraulics*. McGraw-Hill, New York.

Dzafo, H. 2019. "Analysis of the flow with Coanda effect on water intake." Ph.D. thesis, University of Sarajevo, Mechanical Engineering Faculty [*in Bosnian*].

Esmond, S. 2012. "Effectiveness of Coanda Screens for Removal of Sediment, Nutrients, and Metals from Urban Runoff." 43rd International Erosion Control Association Annual Conference 2012, Las Vegas, Nevada, USA, 26-29 February 2012

Finch, H.E., and J. J. Strong. 1983. "Self-cleaning screen." U.S. Patent No. 4,415,462.

Fontein, F. J. 1965. "Some variables influencing sieve-bend performance." *Proceedings, International Chemical Engineers Joint Meeting*, New York.

Gharbi, N. E. 2009. "Effect of near-wall treatments on airflow simulations." Int'l Conf. on Computational Methods for Energy Engineering and Environment: ICCM3E, Susse, Tunisia, 20-22 November, 2009, pp. 185-189.

May, D. 2015. "Sediment Exclusion from Water Systems Using a Coanda Effect Device." *International Journal of Hydraulic Engineering,* 4(2): 23-30. doi: 10.5923/j.ijhe.20150402.01.

Nøvik, H., L. Lia, and H. Opaker. 2014. "Performance of Coanda-effect screens in a cold climate." *Journal of Cold Regions Engineering*, 28(4):04014006. https://doi.org/10.1061/(ASCE)CR.1943-5495.0000073

Strong, J. J., and R. F. Ott. 1988. "Intake Screens for Small Hydro Plants." *Hydro Review*, vol. VII, no. V, October 1988.

Wahl, T. L. 2001. "Hydraulic performance of Coanda-effect screens." *Journal of Hydraulic Engineering*, Vol. 127, No. 6, June 2001, pp. 480-488. https://doi.org/10.1061/(ASCE)0733-9429(2001)127:6(480)

Wahl, T. L. 2003. *Design guidance for Coanda-effect screens*. U.S. Dept. of the Interior, Bureau of Reclamation, Research Report R-03-03. July 2003.

Wahl, T. L. 2013. "New testing of Coanda-effect screen capacities." *HydroVision International 2013*, July 23-26, 2013, Denver, CO.

Pre-print of Wahl et al. (2021). DOI: 10.1061/(ASCE)HY.1943-7900.0001902

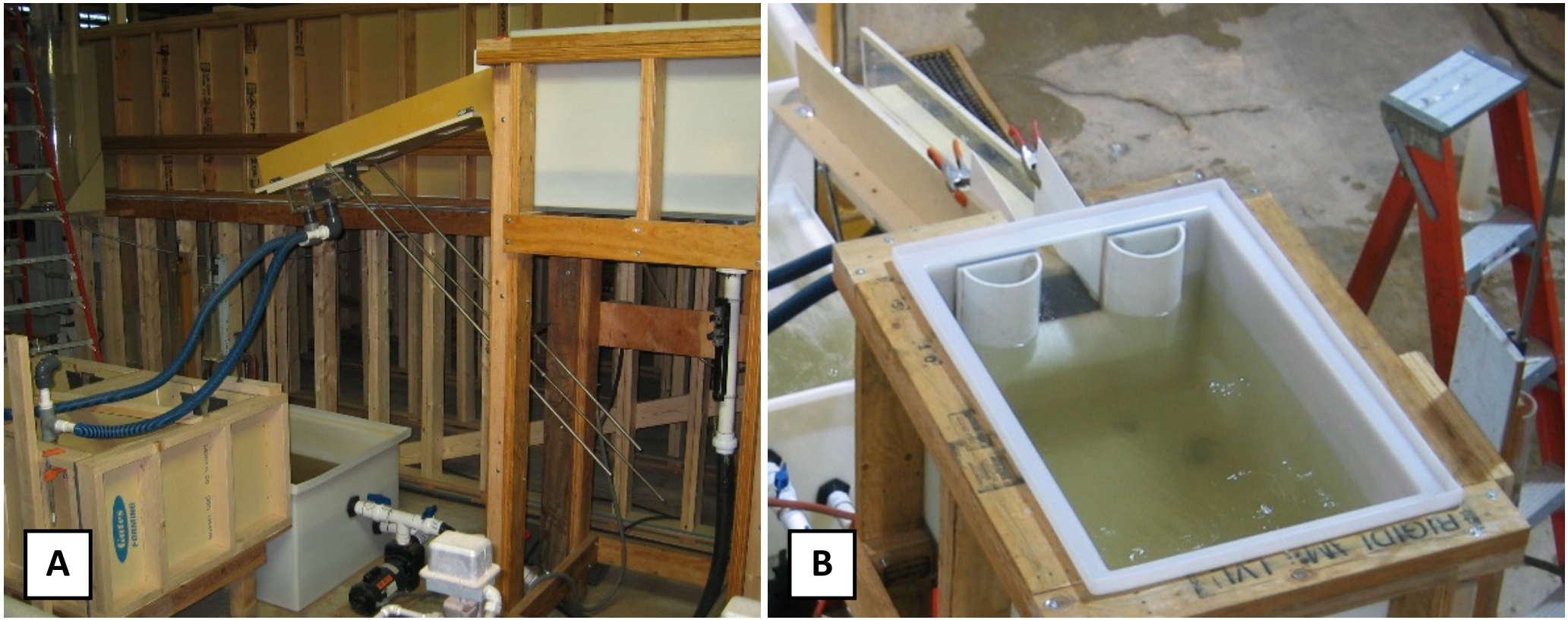

Figure S1. Screen test facility with head tank, flume, tailwater tank and measurement weirs (A), and an overhead view of the head tank and flume entrance (B).

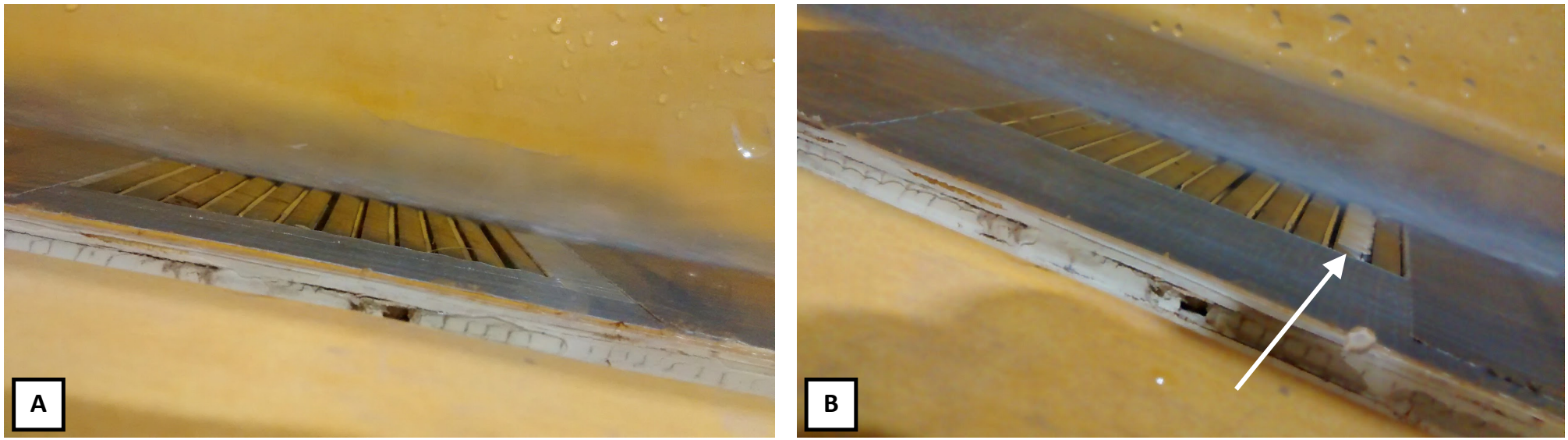

Figure S2. Flow remains attached to the tops of all wires on screen A-8 (A) but skips over the eleventh wire and slot of screen A-6, producing a visible air pocket (B). Flow is left to right in both images.

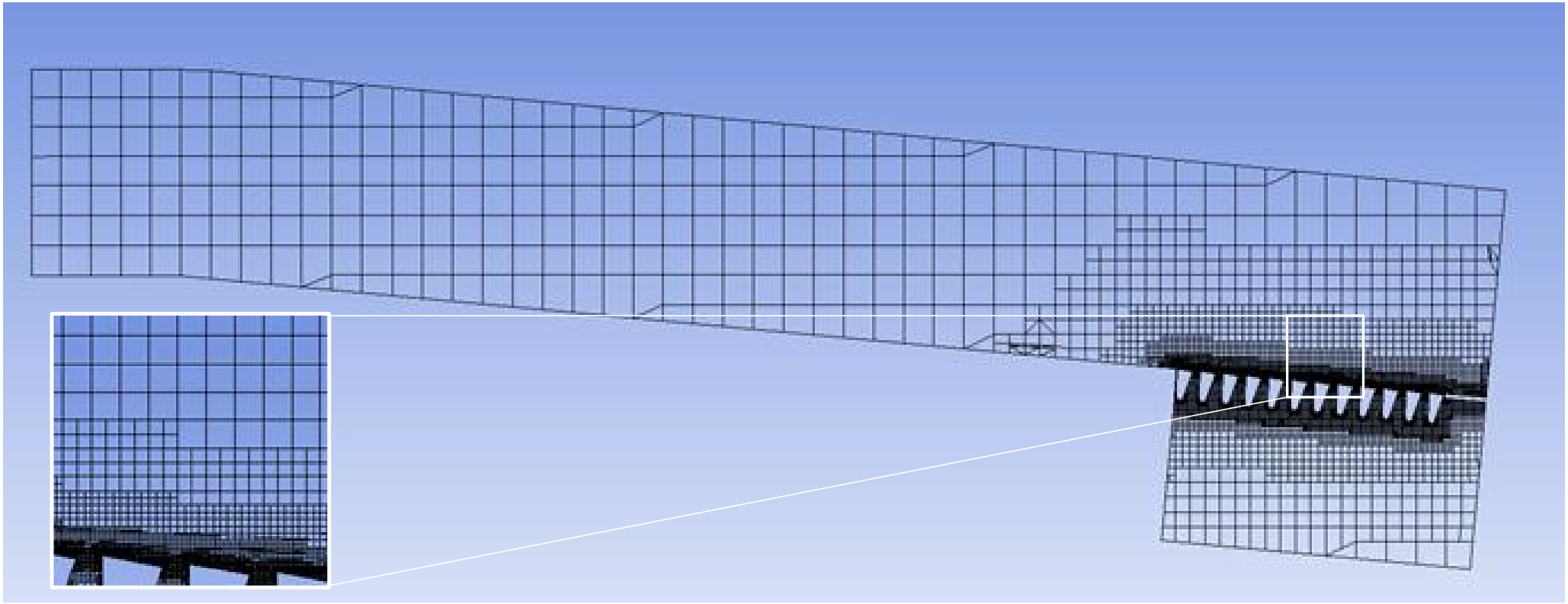

Figure S3. Computational mesh for 2D simulation and detailed mesh around screen wires and slots (inset).

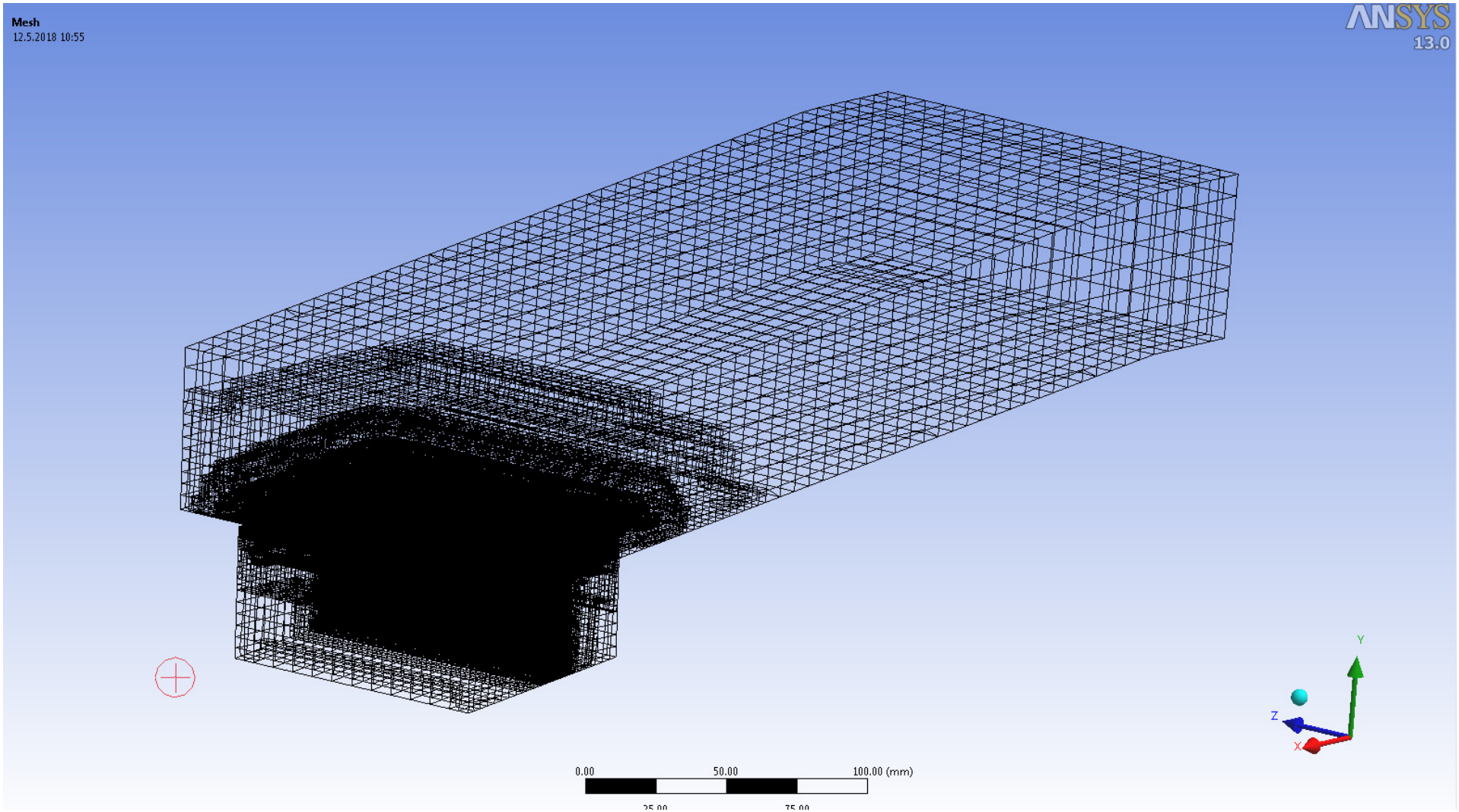

Figure S4. Complete 3D computational mesh with hexahedral cells.

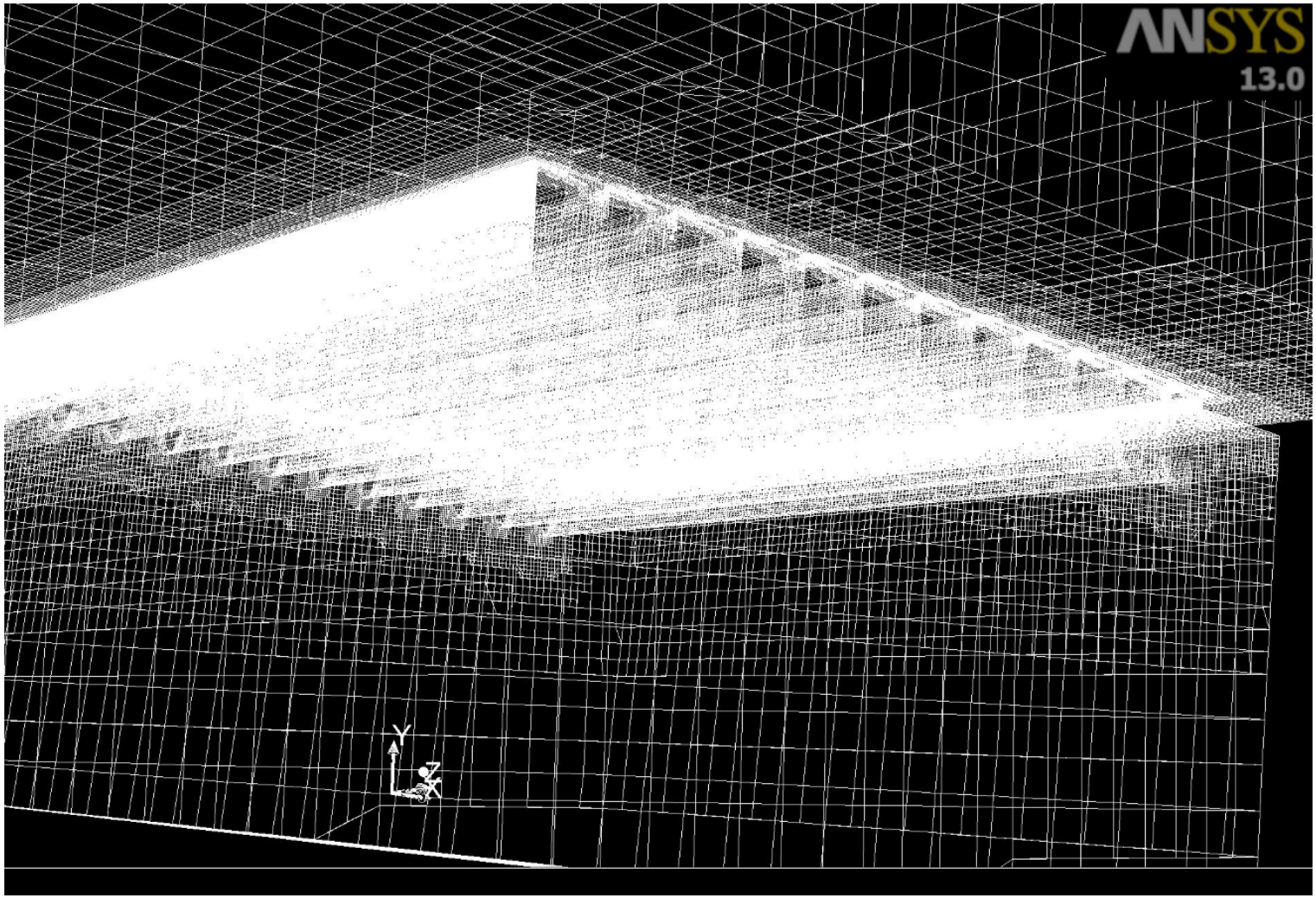

Figure S5. View of 3D computational mesh from beneath a screen panel.

Pre-print of Wahl et al. (2021). DOI: 10.1061/(ASCE)HY.1943-7900.0001902

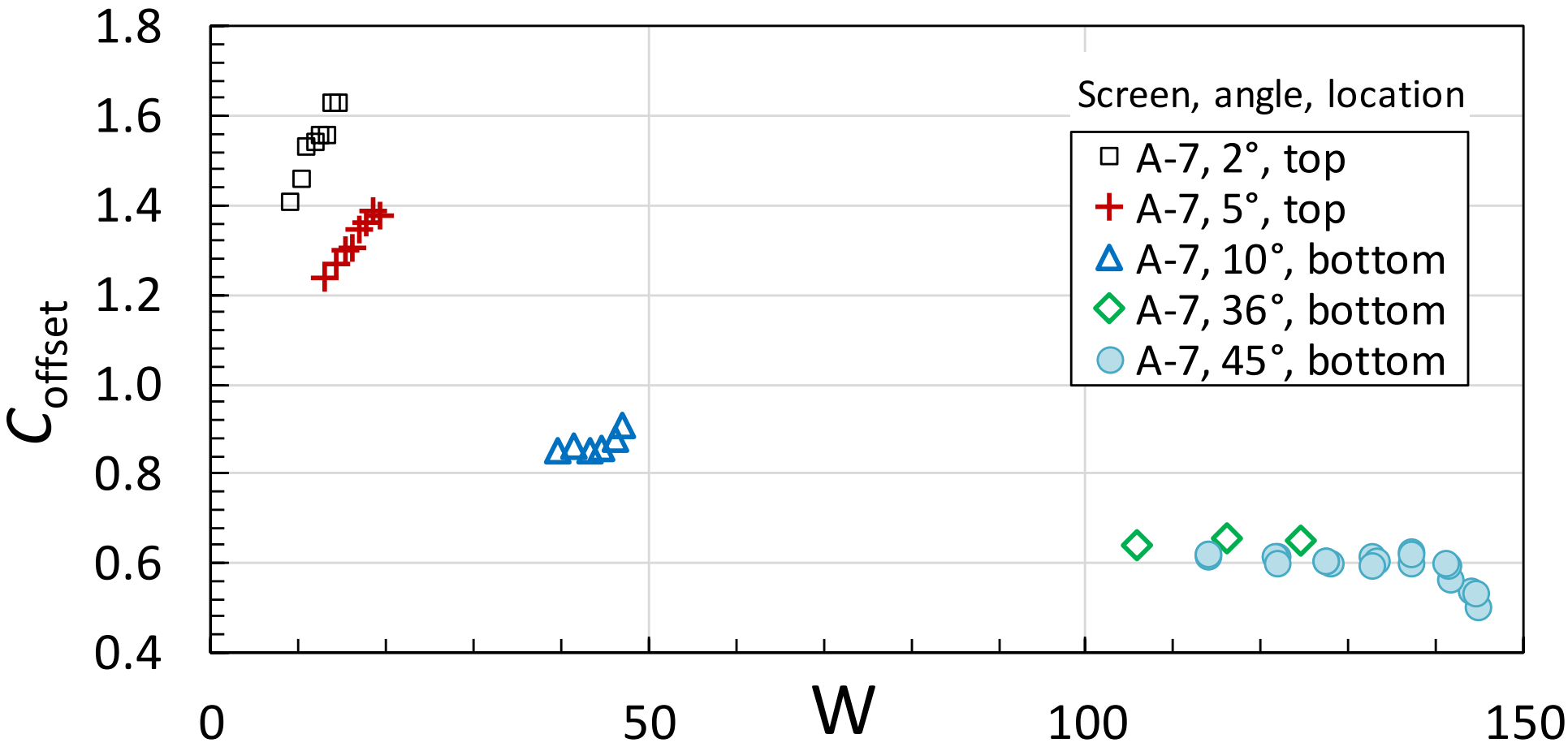

Figure S6. Screen A-7 exhibited a notable reduction of the discharge coefficient at W > 140, presumably due to flow beginning to separate from the screen and skip wires, although it was not noted visually during the tests.